

Measurement of the $e^+e^- \rightarrow \eta\gamma$ cross section near the $\phi(1020)$ resonance with the SND detector

M. N. Achasov,^{1, 2} A. E. Alizzi,^{1, 2} A. Yu. Barnyakov,^{1, 2} E. V. Bedarev,^{1, 2} K. I. Beloborodov,^{1, 2} A. V. Berdyugin,^{1, 2} A. G. Bogdanchikov,¹ A. A. Botov,¹ D. E. Chistyakov,^{1, 2} T. V. Dimova,^{1, 2} V. P. Druzhinin,^{1, 2} L. V. Kardapoltsev,^{1, 2, *} A. S. Kasaev,¹ A. A. Kattsin,¹ A. G. Kharlamov,^{1, 2} I. A. Koop,^{1, 2} A. A. Korol,^{1, 2} D. P. Kovrizhin,¹ A. S. Kupich,^{1, 2} A. P. Kryukov,¹ N. A. Melnikova,¹ N. Yu. Muchnoi,^{1, 2} A. E. Obrazovskiy,¹ A. A. Oorzhak,^{1, 2} E. V. Pakhtusova,¹ I. A. Polomoshnov,^{1, 2} K. V. Pugachev,^{1, 2} S. A. Rastigeev,¹ Yu. A. Rogovsky,^{1, 2} A. I. Senchenko,¹ S. I. Serednyakov,^{1, 2} Yu. M. Shatunov,¹ D. A. Shtol,¹ Z. K. Silagadze,^{1, 2} K. D. Sungurov,^{1, 2, †} I. K. Surin,¹ Yu. V. Usov,¹ V. N. Zhabin,^{1, 2} Yu. M. Zharinov,¹ and V. V. Zhulanov^{1, 2}

¹Budker Institute of Nuclear Physics, SB RAS, Novosibirsk, 630090, Russia

²Novosibirsk State University, Novosibirsk, 630090, Russia

In the experiment with the SND detector at the VEPP-2000 e^+e^- collider, the $e^+e^- \rightarrow \eta\gamma$ cross section is measured in the energy range $E = 980 - 1060$ MeV. The measurement is carried out in the $\eta \rightarrow 2\gamma$ decay mode. Data with an integrated luminosity of 73 pb^{-1} collected in 2018 and 2024 are used in the analysis. The measured cross section is the most accurate to date and is higher compared to other measurements. From the fit to the cross section data with the vector meson dominance model, the value of the product of the branching fractions $B(\phi \rightarrow e^+e^-)B(\phi \rightarrow \eta\gamma)$ has been obtained.

I. INTRODUCTION

Radiative decays of the light vector mesons ρ , ω , ϕ and particularly the decay of the ϕ meson to $\eta\gamma$ are known as a good laboratory for testing various theoretical concepts describing the low-energy QCD dynamics. Their measured decay widths are widely used to test predictions based on the quark model [1, 2] and study the $SU(3)$ flavor symmetry breaking [3]. They are also used to study the $\eta - \eta'$ mixing and the possible admixture of an additional $SU(3)$ singlet state [4–6], which can be attributed to the pseudoscalar glueball predicted by QCD [7] and to the $c\bar{c}$ state [8].

This work is devoted to measurement of the $e^+e^- \rightarrow \eta\gamma$ cross section in the center-of-mass (c.m.) energy range $E = 980 - 1060$ MeV using data collected by the Spherical Neutral Detector (SND) at the e^+e^- collider VEPP-2000. In this energy range, the dominant contribution to the cross section comes from the decay of $\phi \rightarrow \eta\gamma$, which interferes with the tails of $\rho(770)$ and high-lying resonances. The $\phi \rightarrow \eta\gamma$ branching fraction can be obtained from fitting the $e^+e^- \rightarrow \eta\gamma$ cross section within the vector meson dominance (VMD). Near the $\phi(1020)$ resonance, the most accurate measurements of the $e^+e^- \rightarrow \eta\gamma$ cross section were made by the SND [9, 10] and CMD-2 [11–13] experiments at the VEPP-2M collider.

II. SND DETECTOR

The SND detector[14–17] is a general-purpose non-magnetic detector operating at the VEPP-2000 e^+e^- collider [18] with the c.m. energy $E = 0.32 - 2$ GeV. The main part of the SND detector is an electromagnetic calorimeter. The SND calorimeter is made of 1640 NaI(Tl) crystals. It consists of three spherical layers with the total thickness of 13.4 radiation lengths. The calorimeter covers nearly 95% of the full solid angle: $18^\circ \leq \theta \leq 162^\circ$, where θ is the polar angle. The energy resolution of the SND calorimeter is given by the formula $\sigma_E/E_\gamma(\%) = 4.2\%/\sqrt[4]{E_\gamma(\text{GeV})}$, while the angular resolution is $\sigma_\varphi = 0.82^\circ/\sqrt{E_\gamma(\text{GeV})} \oplus 0.63^\circ$. The parameters of charged particles are measured using a nine-layer drift chamber and a proportional chamber with cathode-strip readout located in a common gas volume. Its angular resolution is 0.8° in polar direction, and 0.45° in the azimuthal direction. The solid angle of the tracking system is 94% of 4π . A system of aerogel threshold Cherenkov counters is located around the tracking system. The calorimeter is surrounded by a 10 cm thick iron absorber, behind which there is a muon system consisting of proportional tubes and scintillation counters.

For this work we use data collected by the SND detector at the e^+e^- collider VEPP-2000 in the c.m. energy range $E = 980 - 1060$ MeV. The integrated luminosity accumulated at 21 energy points in 2024 and at 8 energy points in 2018 is about 73 pb^{-1} .

Monte-Carlo (MC) simulation of signal and background processes takes into account radiative corrections [19]. The angular distribution of a hard photon emitted from the initial state is generated according to Ref. [20]. Interactions of the particles produced in e^+e^- annihilation with the detector materials are simulated using the GEANT4 software [21]. The simulation takes into

*Electronic address: l.v.kardapoltsev@inp.nsk.su

†Electronic address: k.d.sungurov@inp.nsk.su

account variation of experimental conditions during data taking, in particular dead detector channels and beam-induced background. To take into account the effect of superimposing the beam background on the e^+e^- annihilation events, the simulation uses special background events recorded during data taking with a random trigger. These events are superimposed on the simulated events, leading to the appearance of additional tracks and photons in them.

The average beam energy and the energy spread were measured during data taking by a dedicated system using the Compton backscattering of laser photons on the electron beam [22]. Energy measurements performed at a given energy point are averaged with weights proportional to the integrated luminosity. The obtained values for average energy, energy spread σ_E and their errors are listed in Table I.

The energy errors listed in Table I describe the relative uncertainties of the measured energy. Additional uncertainty comes from a possible shift of the energy scale. It was estimated to be 60 keV at the c.m. energy $E = 1000$ MeV by comparison with the energy measurement by the resonance depolarization method [22]. Since the measurement of the ϕ meson mass is not a subject of this work, we only need to know the value of this shift relative to the ϕ meson mass (Δm_ϕ). The relative shift of the energy scale for the 2018 energy scan was obtained in Ref. [23] by fitting the energy dependence of the $e^+e^- \rightarrow K_SK_L$ cross section. The measured energies used in Ref. [23] differ slightly from the ones used in this work due to slightly different calibration procedures applied to the data. With the set of measured energies used in this work, the fit of the $e^+e^- \rightarrow K_SK_L$ cross section described in Ref. [23] gives a common shift of all energy points in the 2018 scan $\Delta m_\phi = 0.020 \pm 0.012$ MeV. Taking into account the interaction of K mesons in final state changes it to $\Delta m_\phi^{FSI} = 0.035 \pm 0.012$ MeV. When fitting the energy dependence of the $e^+e^- \rightarrow \eta\gamma$ cross section, we introduce a common energy shift with a Gaussian constraint corresponding to Δm_ϕ^{FSI} . The energy shift Δm_ϕ is used to estimate the associated systematic uncertainty.

We use the $e^+e^- \rightarrow \gamma\gamma$ process to measure the luminosity. For event selection, determination of systematic uncertainties and luminosity corrections, we follow the procedure developed in Ref. [23]. For the coherence with the selection conditions of the $e^+e^- \rightarrow \eta\gamma$ events, we additionally impose selection conditions on the normalized energy deposition in the calorimeter $E_{tot}/E > 0.65$ and on the normalized transverse momentum of the event calculated using the energy depositions in the calorimeter crystals $P_t/E < 0.3$.

The process under study $e^+e^- \rightarrow \eta\gamma \rightarrow 3\gamma$ contains only photons in the final state. The choice of the $e^+e^- \rightarrow \gamma\gamma$ process for the luminosity measurement allows us to cancel systematic uncertainties in the measured cross section that are common to both of these processes. The most important of them are the systematic uncertainties associated with the simulation of the hard-

TABLE I: The center-of-mass energy (E), center-of-mass energy spread (σ_E), and integrated luminosity (IL). For luminosity, the first error is statistical, the second is systematic.

E, MeV	σ_E , keV	IL, nb ⁻¹
2024 energy scan		
980.189 \pm 0.010	470 \pm 97	2061.3 \pm 4.1 \pm 8.9
984.124 \pm 0.012	543 \pm 120	2205.9 \pm 4.2 \pm 7.7
990.032 \pm 0.009	439 \pm 77	1914.7 \pm 4.0 \pm 9.4
1000.039 \pm 0.018	340 \pm 108	4038.3 \pm 5.8 \pm 15.9
1002.038 \pm 0.015	371 \pm 128	1988.8 \pm 4.1 \pm 8.3
1006.034 \pm 0.026	435 \pm 160	2297.2 \pm 4.4 \pm 5.4
1010.091 \pm 0.014	462 \pm 74	2161.9 \pm 4.3 \pm 8.3
1013.099 \pm 0.008	449 \pm 53	2084.7 \pm 4.2 \pm 9.5
1016.110 \pm 0.010	444 \pm 69	3113.8 \pm 5.2 \pm 10.1
1017.073 \pm 0.009	439 \pm 54	3354.9 \pm 5.4 \pm 13.2
1018.111 \pm 0.005	465 \pm 39	3539.2 \pm 5.5 \pm 11.7
1019.073 \pm 0.004	444 \pm 38	4724.9 \pm 6.4 \pm 12.2
1020.055 \pm 0.004	429 \pm 40	4734.9 \pm 6.4 \pm 22.8
1021.005 \pm 0.005	449 \pm 36	3607.3 \pm 5.6 \pm 10.4
1023.079 \pm 0.005	447 \pm 43	3437.3 \pm 5.5 \pm 21.0
1025.003 \pm 0.008	355 \pm 80	2025.1 \pm 4.2 \pm 7.4
1025.058 \pm 0.005	429 \pm 48	2217.0 \pm 4.4 \pm 11.7
1030.072 \pm 0.006	409 \pm 44	2577.1 \pm 4.8 \pm 7.9
1040.047 \pm 0.009	412 \pm 48	2094.0 \pm 4.4 \pm 14.1
1049.992 \pm 0.009	438 \pm 107	4895.1 \pm 6.8 \pm 22.0
1060.206 \pm 0.012	444 \pm 56	599.9 \pm 2.4 \pm 3.6
2018 energy scan		
1005.999 \pm 0.021	359 \pm 39	1681.6 \pm 3.8 \pm 4.8
1016.843 \pm 0.023	351 \pm 64	1650.1 \pm 3.7 \pm 3.0
1017.959 \pm 0.023	375 \pm 84	1256.4 \pm 3.3 \pm 3.5
1019.101 \pm 0.019	380 \pm 36	2454.3 \pm 4.6 \pm 7.2
1019.982 \pm 0.019	380 \pm 61	2640.2 \pm 4.8 \pm 9.7
1020.932 \pm 0.046	406 \pm 26	1424.4 \pm 3.5 \pm 3.0
1022.114 \pm 0.030	372 \pm 36	1229.1 \pm 3.2 \pm 4.8
1022.929 \pm 0.041	382 \pm 43	821.3 \pm 2.7 \pm 1.2

ware first-level trigger and the superimposition of beam-generated spurious tracks onto signal events. For this reason, we do not apply the correction on the superimposition of beam-generated tracks introduced in Ref. [23].

The resulted integrated luminosity for each energy point is presented in Table I with statistical and systematic errors. The systematic uncertainty does not exceed 0.6%.

III. SELECTION OF $e^+e^- \rightarrow \eta\gamma$ EVENTS

The selection of $e^+e^- \rightarrow \eta\gamma$ events is performed in two stages. At the first stage, we select events with at least 3 photons with energies above 20 MeV, without charged tracks, $E_{tot}/E > 0.65$ and $P_t/E < 0.3$. For events pass-

ing these selection conditions, we perform a kinematic fit to the $e^+e^- \rightarrow 3\gamma$ hypotheses with the requirements of energy and momentum conservation. For kinematic fit, we choose only those photons in the event which have energy $E_\gamma > 50$ MeV and polar angle $27^\circ < \theta_\gamma < 153^\circ$. If the number of photons in an event that meets these conditions is less than 3 or more than 8, then such event is discarded. As a result of the kinematic fit, the energies and angles of photons are refined, and the χ^2 of the $e^+e^- \rightarrow 3\gamma$ kinematic hypothesis is calculated ($\chi^2_{3\gamma}$). In the kinematics fitting, all possible combinations of photons are tested, and the combination with the smallest χ^2 value is retained. For further analysis, we use the refined values of photon angles and energies, and impose the following selection condition on obtained χ^2 of the kinematic fit $\chi^2_{3\gamma} < 30$.

To reconstruct the invariant mass of two photons from the η meson decay ($M_{\gamma\gamma}$), we employ the procedure described in Ref. [13]. The photon energies refined after kinematic fit are sorted in descending order $E_1 > E_2 > E_3$. If $E_3 < m_\eta^2/E$, then $M_{\gamma\gamma} = \sqrt{4E_b(E_b - E_2)}$, otherwise $M_{\gamma\gamma} = \sqrt{4E_b(E_b - E_1)}$. Here m_η is the η meson mass and $E_b = E/2$. The following constraint is imposed on the obtained invariant mass $350 < M_{\gamma\gamma} < 700$ MeV.

The dominant background for this analysis arises from the QED process of e^+e^- annihilation to 3 photons. For an accurate description of the background, it is also important to take into account the annihilation into 2 photons with an additional photon from the splitting of the electromagnetic shower or beam background, and the annihilation into four and more photons. To model these processes, we generate a sample of the $e^+e^- \rightarrow \gamma\gamma(\gamma)$ events using the Monte Carlo event generator BabaYaga@NLO [24]. For $e^+e^- \rightarrow 2\gamma, 3\gamma$, it exploits the exact amplitude up to the $\mathcal{O}(\alpha^3)$ contributions. In addition to this, it models the emission of an arbitrary number of additional photons using the QED Parton Shower algorithm.

The main hadronic background, which also gives a three-photon final state, is the $e^+e^- \rightarrow \pi^0\gamma$ process. In addition to it, we also study the contribution to the background from the hadronic processes with multiphoton final state $e^+e^- \rightarrow K_SK_L$, $e^+e^- \rightarrow 2\pi^0\gamma$, $e^+e^- \rightarrow \eta\gamma \rightarrow 3\pi^0\gamma$. The cosmic ray background is studied by analysing the event time measured in the electromagnetic calorimeter and found to be negligible.

Figure 1 shows the $\chi^2_{3\gamma}$ distribution for data and MC simulation at $E = 1020.055$ MeV after applying the selection conditions. All distributions for the MC simulation are normalized to the expected number of events. The shares of their contributions to the signal region $\chi^2_{3\gamma} < 30$ is following: $e^+e^- \rightarrow \eta\gamma \rightarrow 3\gamma$ - 60.0%, QED processes - 26.1%, $e^+e^- \rightarrow \pi^0\gamma$ - 12.4%, multiphoton hadronic processes - 1.4%. Since the $e^+e^- \rightarrow \gamma\gamma(\gamma)$ and $e^+e^- \rightarrow \pi^0\gamma$, as well as the studied process $e^+e^- \rightarrow \eta\gamma \rightarrow 3\gamma$, have three photons in the final state, their $\chi^2_{3\gamma}$ distributions have a peak at low values of $\chi^2_{3\gamma}$. For this reason, these processes give the dominant contribution to the back-

ground in the signal region.

IV. FITTING THE $M_{\gamma\gamma}$ DISTRIBUTION

The $M_{\gamma\gamma}$ distributions for the energy points corresponding to the maximum of the $\phi(1020)$ resonance and its left and right tails are shown in Fig. 2. To determine the number of signal events (N_{sig}) at each energy point, we perform a binned likelihood fit to the $M_{\gamma\gamma}$ distribution with a sum of signal (F_{sig}) and background (F_{bkg}) distributions. The background distribution is composed of two components F_{bkg}^I and F_{bkg}^{II} . The distributions F_{bkg}^I and F_{bkg}^{II} are shown in Fig. 2 as stacked histograms. They content background events with $E_3 < m_\eta^2/E$ and $E_3 > m_\eta^2/E$, respectively.

The signal distribution is obtained by fitting the mass spectra for the simulated signal events by a sum of three Gaussian functions. When fitting the data, the F_{sig} function obtained from the simulation is modified to account for possible difference between the data and the simulation in the detector response. A common mass shift ΔM and a smearing $\Delta\sigma^2$ are added to each Gaussian mean and variance, respectively, in the following way: $M_{\gamma\gamma}^{data} = M_{\gamma\gamma}^{MC} + \Delta M$ and $\sigma_{data}^2 = \sigma_{MC}^2 + \Delta\sigma^2$. The values of ΔM and $\Delta\sigma^2$ are determined by fitting the data $M_{\gamma\gamma}$ distributions in the energy region $E = 1017 - 1023$ MeV. They are found to be $\Delta M = -0.77 \pm 0.05$ (-0.42 ± 0.08) MeV and $\Delta\sigma^2 = 1.11 \pm 1.18$ (1.21 ± 1.88) MeV 2 for the 2024 (2018) energy scan. The parameters ΔM and $\Delta\sigma^2$ are fixed at these values. The variation of these parameters within the errors is used to estimate the associated sys-

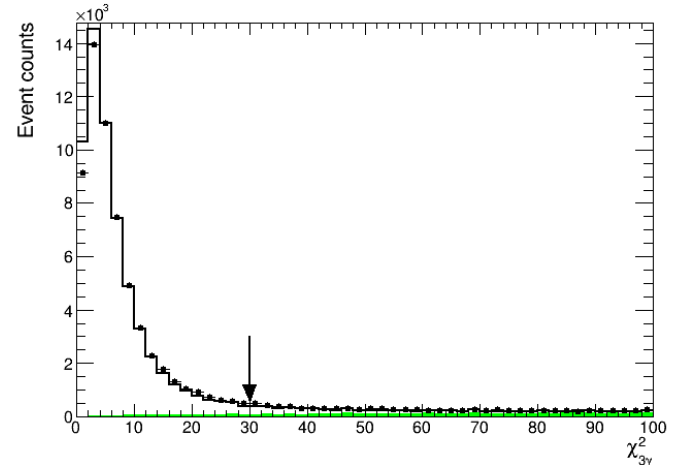


FIG. 1: The distribution of $\chi^2_{3\gamma}$ at $E = 1020.055$ MeV for the data (dots with error bars) and simulation of the signal and the background processes (open histogram). The shaded histogram represents the contribution of the multiphoton hadronic background. The simulated distributions are normalized to the number of expected events. The arrow indicates the boundary of the selection condition.

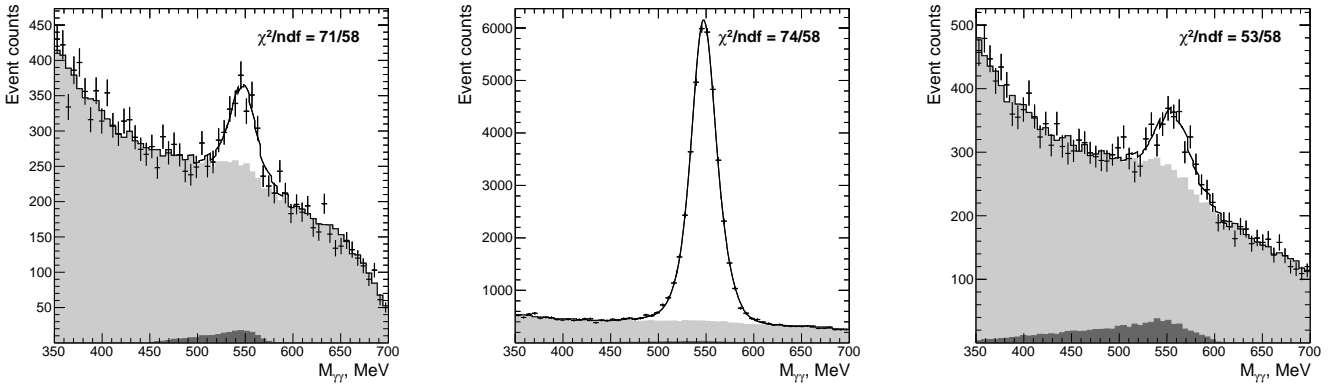


FIG. 2: The $M_{\gamma\gamma}$ distribution for data events (points with error bars) at $E = 1000.039$ MeV (left), $E = 1020.055$ MeV (middle), $E = 1049.992$ MeV (right). The solid curve represents the result of the fit described in the text. The background distribution is shown as stacked histograms for F_{bkg}^I (in light gray) and F_{bkg}^{II} (in dark gray).

tematic uncertainty.

The background distributions F_{bkg}^I and F_{bkg}^{II} are described by histograms obtained from simulation of background processes $e^+e^- \rightarrow \gamma\gamma(\gamma)$, $e^+e^- \rightarrow \pi^0\gamma$, $e^+e^- \rightarrow K_SK_L$, $e^+e^- \rightarrow 2\pi^0\gamma$ and $e^+e^- \rightarrow \eta \rightarrow 3\pi^0\gamma$. To model possible inaccuracies of such a description, we introduce two additional parameters α and β and parametrize the background distribution F_{bkg} as follows

$$F_{bkg} = \alpha [\beta \cdot F_{bkg}^I + ((1 - \beta) \cdot D + 1) \cdot F_{bkg}^{II}], \quad (1)$$

where D is the ratio of numbers of expected events in F_{bkg}^I and F_{bkg}^{II} . The parameters α and β model the possible inaccuracy of MC predictions for the number of background events and parameter D , respectively. The values of parameters $\alpha = 1$ and $\beta = 1$ correspond to the expected background distribution.

Usually, the photon with the misreconstructed energy has the lowest energy out of the three photons selected for the kinematic fitting. Since we choose a pair of photons for $M_{\gamma\gamma}$ depending on the energy of this photon E_3 , we cannot fully rely on simulation to determine the parameter D . Instead, the parameter β is determined by fitting the data $M_{\gamma\gamma}$ distributions in the energy region out of the $\phi(1020)$ resonance peak $E = 980 - 1013$ MeV and $E = 1025 - 1060$ MeV. For all energy points from this region, the obtained values for the parameter β are consistent with unity. When we determine N_{sig} , the parameter β is fixed at its average value $\beta = 1.000 \pm 0.004$ and its error is used to estimate the associated systematic uncertainty. The parameter α is set to be free. The obtained values for it have no visible energy dependence. Its average value is $\alpha = 0.984 \pm 0.003$.

The results of the fit for three energy points are shown in Fig. 2. The fit quality is reasonably good in the whole studied c.m. energy range. The procedure of choosing a pair of photons for $M_{\gamma\gamma}$ notably distorts the background distribution mostly because the F_{bkg}^{II} distribution looks like a bump at the η meson mass (Fig. 2). The possible

inaccuracy of modeling this distortion is parametrized by the parameter β and gives the dominant contribution to the systematic uncertainty in N_{sig} .

The obtained numbers of signal events for each energy point are listed in Table III with statistical and systematic errors. The systematic error is obtained by variation of the parameters ΔM , $\Delta\sigma^2$ and β within their errors.

V. DETECTION EFFICIENCY

The detection efficiency of $e^+e^- \rightarrow \eta\gamma \rightarrow 3\gamma$ events is determined using MC simulation as a function of E and $x = 2E_r/E$, where E_r is the energy of the extra photon emitted from the initial state. It is parametrized as $\varepsilon_r(E, x) = \varepsilon_0(E)g(E, x)$, where $\varepsilon_0(E) = \varepsilon_r(E, 0)$ and $g(E, 0) = 1$. Since the studied energy region is narrow, the dependence of g on E can be neglected. In this case, all variations of the experimental conditions (dead calorimeter channels, beam background, etc.) are accounted for in $\varepsilon_0(E)$. The dependence of g on x is obtained using MC simulation and then approximated by a smooth function. The result of the approximation is shown in Fig. 3. The decrease of the efficiency at $x = 0.1 - 0.3$ is due to the requirement of energy and momentum balance in an event (the condition $\chi_{3\gamma}^2 < 30$). The increase near the maximum allowed value of x corresponds to the radiative return to the threshold of the reaction $e^+e^- \rightarrow \eta\gamma$ when the photon recoiling against the η meson becomes soft. The initial state radiation photon together with two photons from the η decay provide a good energy-momentum balance, and such an event passes the selection conditions. In spite of this, the number of events from this kinematic region is negligible due to the low probability of emitting a hard photon and the very small $e^+e^- \rightarrow \eta\gamma$ cross section near the threshold.

The imperfect MC simulation of the detector response for photons leads to an inaccuracy in the detection efficiency determined using the MC simulation. To evaluate

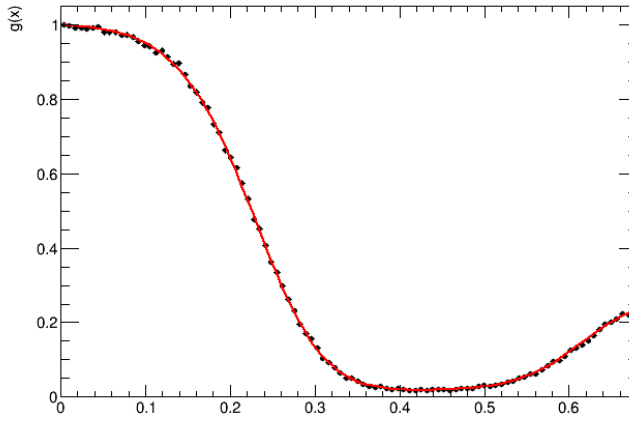


FIG. 3: The x dependence of the detection efficiency obtained from simulation is shown by points with error bars. The solid curve is the result of approximation by a smooth function.

the efficiency corrections, we vary the boundaries of the selection conditions. The correction is defined as a double ratio $1 + \delta_{cut} = (N^{data}/N^{MC})/(N_0^{data}/N_0^{MC})$, where N^{data} (N_0^{data}) and N^{MC} (N_0^{MC}) are the number of signal events in the data and in the signal MC simulation, respectively, for the modified (baseline) selection condition. With the correction defined in this way, the corrected efficiency ε_0 is related to the efficiency obtained from the MC simulation ε_0^{MC} as follows $\varepsilon_0 = \varepsilon_0^{MC}/(1 + \delta_{cut})$.

To estimate the systematic uncertainty associated with the condition on the polar angle of photons accepted for the kinematic fit ($\theta_0 < \theta_\gamma < 180^\circ - \theta_0$ with $\theta_0 = 27^\circ$), we change θ_0 to 36° and 45° . The step of the θ_0 variation corresponds to the angular size of the calorimeter crystal. The signal efficiency decreases by 28 (50)% for $\theta_0 = 36^\circ(45^\circ)$, while the maximum deviation of the correction obtained for the different θ_0 does not exceed 0.6%. This deviation is taken as an estimate of the systematic uncertainty due to the condition on the photon polar angle.

The fraction of signal events rejected by the condition $\chi_{3\gamma}^2 < 30$ is 7.7% at the maximum of the $\phi(1020)$ resonance. When the selection condition is relaxed to $\chi_{3\gamma}^2 < 100$ (800), the fraction of rejected events decreases to 3.0% (0.1%). To evaluate the efficiency correction, we relax the condition from $\chi_{3\gamma}^2 < 30$ to $\chi_{3\gamma}^2 < 800$ and impose additional constraints requiring exactly three photons in an event and no signal in the muon system. In a signal event with $\chi_{3\gamma}^2 > 100$, typically at least one photon hits the dead counter of the electromagnetic calorimeter. This leads to a misreconstruction of the photon energy and, as a consequence, to an incorrect reconstruction of the kinematics of the entire event. For this reason, the peak at the η meson mass in the $M_{\gamma\gamma}$ distribution becomes very broad, making it impossible to separate the signal events from the background. At the same time,

the angles of such photons are measured with sufficient accuracy. To improve the resolution of the reconstructed η meson mass for events with $\chi_{3\gamma}^2 > 100$, we perform a special kinematic fit using only the measured photon angles and ignoring their measured energies. The variation of the correction when changing the condition on $\chi_{3\gamma}^2$ from 100 to 800 is taken as a systematic uncertainty. The efficiency correction is determined at each energy point in the energy range $E = 1017 - 1023$ MeV. For the 2024 energy scan δ_{χ^2} does not depend on energy point and its value is $\delta_{\chi^2} = 1.2 \pm 0.3$ %. For the 2018 energy scan δ_{χ^2} varies from -1.1 % to 3.0 % with systematic uncertainty estimated to be 0.6 %.

A photon converted in the material before the tracking system is reconstructed as a charged track. Since events with charged tracks are rejected by our selection conditions, the data-MC simulation difference in the conversion probability leads to a systematic shift in the measured cross section. This difference was studied in Ref. [23], where the conversion probability was found to be greater than in the simulation by $(0.23 \pm 0.02)/\sin\theta_\gamma$, where θ_γ is the photon polar angle. The efficiency correction for the process $e^+e^- \rightarrow \gamma\gamma$ is calculated to be (0.53 ± 0.04) % and was applied to the measured luminosity. The correction for the process $e^+e^- \rightarrow \eta\gamma$ is calculated to be $\delta_{conv} = (0.86 \pm 0.06)$ %.

The corrected detection efficiencies ε_0 are listed in Table III.

VI. FITTING THE MEASURED CROSS SECTION

The visible cross section of the process $e^+e^- \rightarrow \eta\gamma$ is determined as

$$\sigma_{vis}(E) = \frac{N_{sig}}{IL \cdot B(\eta \rightarrow 2\gamma)}, \quad (2)$$

where IL is the integrated luminosity and $B(\eta \rightarrow 2\gamma) = 39.36 \pm 0.18$ % [25]. It is related to the Born cross section

TABLE II: Results of the fit described in the text.

Parameter	Solution 1	Solution 2	Solution 3
σ_ϕ , nb	$60.69^{+0.36}_{-0.39}$	$56.39^{+0.35}_{-0.31}$	$57.24^{+0.42}_{-0.50}$
φ_ϕ , deg.	192 ± 6	124 ± 5	150 ± 8
$\sigma_{\rho'}$, pb	$3.6^{+3.0}_{-2.2}$	$1.5^{+2.2}_{-1.5}$	$28.5^{+6.6}_{-6.8}$
$\sigma_{\phi'}$, pb	$5.4^{+8.7}_{-3.5}$	$4.6^{+6.2}_{-3.0}$	$3.5^{+2.7}_{-3.5}$
$\varphi_{\rho'}$, deg.	28 ± 31	39 ± 28	-103 ± 9
ΔE_{18} , keV	40 ± 10	41 ± 10	40 ± 10
ΔE_{24} , keV	-213 ± 15	-208 ± 15	-211 ± 14
χ^2/ndf	$35.2/37$	$37.4/37$	$37.6/37$

$\sigma(E)$ as follows:

$$\sigma_{vis}(E) = \int_0^{x_{max}} \varepsilon_0(E)g(E, x)F(x, E)\sigma(E\sqrt{1-x})dx , \quad (3)$$

where $F(x, E)$ is a so-called radiator function [19] describing the probability to emit an extra photon with the total energy $xE/2$ from the initial state, $x_{max} = 1 - m_\eta^2/E^2$. The expression (3) can be rewritten in the conventional form:

$$\sigma_{vis}(E) = \varepsilon_0(E)\sigma(E)(1 + \delta(E)) , \quad (4)$$

To take into account the beam energy spread, it is necessary to perform a convolution of the visible cross section (4) with a Gaussian function describing the c.m. energy distribution of the electron-positron pair. Since the energy spread is much smaller than the width of the $\phi(1020)$ resonance, we use an approximate expression for the convolution

$$\begin{aligned} \sigma_{vis}(E) &\implies \sigma_{vis}(E) + \frac{1}{2} \frac{d^2\sigma_{vis}}{dE^2}(E)\sigma_E^2 \\ &= \sigma_{vis}(E)(1 + \delta_E(E)) \end{aligned} \quad (5)$$

The uncertainty in the collider energy listed in Table I effectively increases the uncertainty in the measured visible cross section. When fitting the cross section energy dependence, the following term is added in quadrature to the statistical error of σ_{vis} :

$$\delta E \frac{d\sigma_{vis}}{dE}(E) , \quad (6)$$

where δE is the uncertainty of the energy measurement of the corresponding energy point. In the energy range $E = 1016 - 1023$ MeV, this additional uncertainty is comparable to the statistical error.

Energy dependence of the $e^+e^- \rightarrow \eta\gamma$ Born cross section is described using the vector meson dominance model, which, in addition to the dominant amplitude of the ϕ meson, includes the amplitudes of the ρ and ω mesons as well as amplitudes describing the contribution of the high-lying vector resonances $\rho(1450)$ (ρ') and $\phi(1680)$ (ϕ'):

$$\sigma_{\eta\gamma}(E) = \frac{q(E)^3}{E^3} \left| \sum_{V=\rho,\omega,\phi,\rho',\phi'} A_V(E) \right|^2 , \quad (7)$$

$$A_V(E) = \frac{m_V \Gamma_V e^{i\varphi_V}}{D_V(E)} \sqrt{\frac{m_V^3}{q(m_V)^3} \sigma_V} , \quad (8)$$

$$D_V(E) = m_V^2 - E^2 - iE\Gamma_V(E) , \quad (9)$$

$$q(E) = \frac{E}{2} \left(1 - \frac{m_\eta^2}{E^2} \right) , \quad (10)$$

where m_V is the resonance mass, $\Gamma_V(E)$ is its energy-dependent total width ($\Gamma_V \equiv \Gamma_V(m_V)$), σ_V is the Born cross section of the process $e^+e^- \rightarrow V \rightarrow \eta\gamma$ at $E = m_V$, φ_V are interference phases relative to the ρ meson ($\varphi_\rho \equiv 0$).

The quark model predicts $\varphi_\omega = 0^\circ$ and $\varphi_\phi = 180^\circ$ [26], which agrees well with measurements [10]. Assuming that the resonances $\rho(1450)$ and $\phi(1680)$ belong to the same 2^3S_1 nonet and taking into account the lattice QCD predictions of their almost ideal mixing [27], we can expect the same pattern for their relative phases. For these reasons, the phase between the ρ and ω mesons is fixed at $\varphi_\omega = 0^\circ$, and $\varphi_{\phi'} = \varphi_\rho + 180^\circ$.

To determine the contribution of high-lying vector resonances, the cross section measured by SND [28] in the energy range $E = 1070 - 2000$ MeV is added to the fit. The masses and widths of all vector resonances are fixed at their PDG values [25]. The parameters σ_ρ and σ_ω are fixed at the values taken from the SND measurement [10],

$$\sigma_\rho = (0.322 \pm 0.0034 \pm 0.019) \text{ nb} , \quad (11)$$

$$\sigma_\omega = (0.744 \pm 0.075 \pm 0.027) \text{ nb} . \quad (12)$$

The free fit parameters are σ_ϕ , φ_ϕ , $\sigma_{\rho'}$, $\varphi_{\rho'}$, $\sigma_{\phi'}$ and the shifts of the energy scale for the 2024 scan ΔE_{24} and for the 2018 scan ΔE_{18} . As was discussed above, the parameter ΔE_{18} is constrained by a Gaussian penalty term corresponding to $\Delta m_\phi^{FSI} = 0.035 \pm 0.012$ MeV. To evaluate the systematic uncertainty associated with the energy scale, the constraint in penalty term is changed to $\Delta m_\phi = 0.020 \pm 0.012$ MeV.

The result of the fit is presented in Table II and shown in Fig. 4. We found three different solutions with very close and good fit quality $\chi^2/ndf = (35-38)/37$, where ndf is the number of degrees of freedom. This is a consequence of the well-known problem that the interfering Breit-Wigner resonances have ambiguities in the determination of their parameters [29]. As discussed above, the quark model predicts the relative phase $\varphi_\phi = 180^\circ$. The only first solution presented in Table II has relative phase φ_ϕ compatible with this value. For this reason, we choose it as a nominal one. We use this solution for all calculations with the theoretical model, unless otherwise explicitly stated. It is also worth noting that in both experimental works, where the contribution of $\rho(1450)$ was taken into account [10, 13], the phase was fixed at $\varphi_{\rho'} = 0^\circ$.

The results of the fit are used to calculate the radiative correction and the energy spread correction. The difference between the corrections obtained with different fit solutions is considerable only for two energy points with $E = 1049.992$ MeV and 1060.206 MeV. For them, this difference is 1.5% and 4%, respectively, and is taken as systematic uncertainty. The value of the Born cross section at a given energy point is determined as follows

$$\sigma = \frac{N_{sig}}{\varepsilon_0 IL(1 + \delta)(1 + \delta_E)B(\eta \rightarrow 2\gamma)} . \quad (13)$$

TABLE III: The center-of-mass energy (E), detection efficiency (ε_0), number of signal events (N_{sig}), radiative correction ($1 + \delta$), correction for the energy spread ($1 + \delta_E$), Born cross section for the process $e^+e^- \rightarrow \eta\gamma$ (σ). The first error in the number of events and cross section is statistical, the second is systematic.

E , GeV	ε_0 , %	N_{sig}	$1 + \delta$	$1 + \delta_E$	σ , nb
2024 energy scan					
980.189	53.4	$155 \pm 42 \pm 23$	0.881	1.000	$0.41 \pm 0.11 \pm 0.06$
984.124	53.1	$238 \pm 44 \pm 24$	0.872	1.000	$0.59 \pm 0.11 \pm 0.06$
990.032	53.0	$161 \pm 41 \pm 17$	0.856	1.000	$0.47 \pm 0.12 \pm 0.05$
1000.039	52.7	$712 \pm 62 \pm 33$	0.823	1.001	$1.03 \pm 0.09 \pm 0.05$
1002.038	53.3	$537 \pm 47 \pm 16$	0.815	1.001	$1.58 \pm 0.14 \pm 0.05$
1006.034	53.3	$769 \pm 51 \pm 17$	0.797	1.002	$2.00 \pm 0.13 \pm 0.05$
1010.091	53.6	$1376 \pm 57 \pm 15$	0.774	1.006	$3.88 \pm 0.16 \pm 0.06$
1013.099	53.0	$2377 \pm 67 \pm 16$	0.752	1.011	$7.19 \pm 0.21 \pm 0.09$
1016.110	52.6	$10372 \pm 121 \pm 27$	0.726	1.022	$21.68 \pm 0.29 \pm 0.27$
1017.073	52.9	$16651 \pm 149 \pm 32$	0.719	1.018	$32.55 \pm 0.37 \pm 0.37$
1018.111	53.3	$26770 \pm 183 \pm 36$	0.719	0.988	$50.71 \pm 0.45 \pm 0.53$
1019.073	52.6	$41526 \pm 225 \pm 50$	0.740	0.960	$59.79 \pm 0.44 \pm 0.75$
1020.055	52.9	$36168 \pm 212 \pm 46$	0.790	0.990	$46.89 \pm 0.40 \pm 0.49$
1021.005	52.8	$19774 \pm 159 \pm 31$	0.863	1.015	$30.13 \pm 0.31 \pm 0.32$
1023.079	51.7	$8694 \pm 112 \pm 22$	1.055	1.016	$11.60 \pm 0.17 \pm 0.13$
1025.003	51.9	$2925 \pm 70 \pm 12$	1.257	1.006	$5.59 \pm 0.14 \pm 0.06$
1025.058	52.0	$3354 \pm 74 \pm 12$	1.263	1.008	$5.81 \pm 0.14 \pm 0.06$
1030.072	52.5	$1568 \pm 61 \pm 12$	1.871	1.003	$1.570 \pm 0.069 \pm 0.020$
1040.047	52.7	$518 \pm 47 \pm 8$	3.477	1.001	$0.343 \pm 0.036 \pm 0.006$
1049.992	52.4	$713 \pm 69 \pm 15$	5.672	1.000	$0.124 \pm 0.017 \pm 0.004$
1060.206	53.2	$84 \pm 25 \pm 2$	8.505	1.000	$0.079 \pm 0.025 \pm 0.004$
2018 energy scan					
1005.999	52.9	$598 \pm 44 \pm 10$	0.797	1.002	$2.14 \pm 0.16 \pm 0.04$
1016.843	52.5	$6482 \pm 95 \pm 15$	0.722	1.014	$25.97 \pm 0.48 \pm 0.33$
1017.959	51.2	$7711 \pm 100 \pm 12$	0.718	1.003	$42.30 \pm 0.72 \pm 0.49$
1019.101	52.6	$20990 \pm 161 \pm 27$	0.732	0.972	$58.02 \pm 0.55 \pm 0.74$
1019.982	52.8	$21546 \pm 163 \pm 26$	0.770	0.982	$51.91 \pm 0.55 \pm 0.67$
1020.932	52.4	$8747 \pm 105 \pm 12$	0.836	1.008	$35.36 \pm 0.80 \pm 0.41$
1022.114	51.7	$4744 \pm 80 \pm 9$	0.938	1.012	$19.96 \pm 0.43 \pm 0.23$
1022.929	53.0	$2343 \pm 58 \pm 5$	1.015	1.013	$13.31 \pm 0.40 \pm 0.16$

The values of $(1 + \delta)$, $(1 + \delta_E)$ and the Born cross sections with statistical and systematic errors are listed in Table III. The main contributions to the systematic uncertainty come from the uncertainties in the luminosity measurement (0.6%), the condition on the polar angle of photons (0.6%), the condition on $\chi^2_{3\gamma}$ of the kinematic reconstruction (0.3-0.6%), the accuracy of $B(\eta \rightarrow 2\gamma)$ (0.5%) and the energy spread correction. The latter is due to the uncertainty in the measurement of σ_E and reaches 0.7% for the energy point with $E = 1019.073$ MeV. At the tails of the $\phi(1020)$ resonance the systematic uncertainty is dominated by the uncertainty of the number of signal events (up to 15%). The total systematic uncertainty is obtained as a sum in quadrature of all systematic uncertainties from different sources. It varies from 1% to 15% depending on the energy point and is

comparable to the statistical error at the vicinity of the $\phi(1020)$ resonance maximum.

The obtained energy scale shift for the 2024 scan ΔE_{24} (Table II) significantly exceeds its systematic uncertainty (60 keV) estimated in Ref. [22]. Although the origin of such a shift is unclear, it does not affect the measured cross section.

The obtained values of the Born cross sections are actually numerical solutions of the integral equation (3), in which the theoretical model is used for regularization. Since the theoretical model is the same for all energy points, the Born cross sections obtained for different energy points can be correlated. To study these correlations, a series of 10^4 pseudoexperiments is used. The number of signal events for each energy point is generated according to the theoretical model with a variance

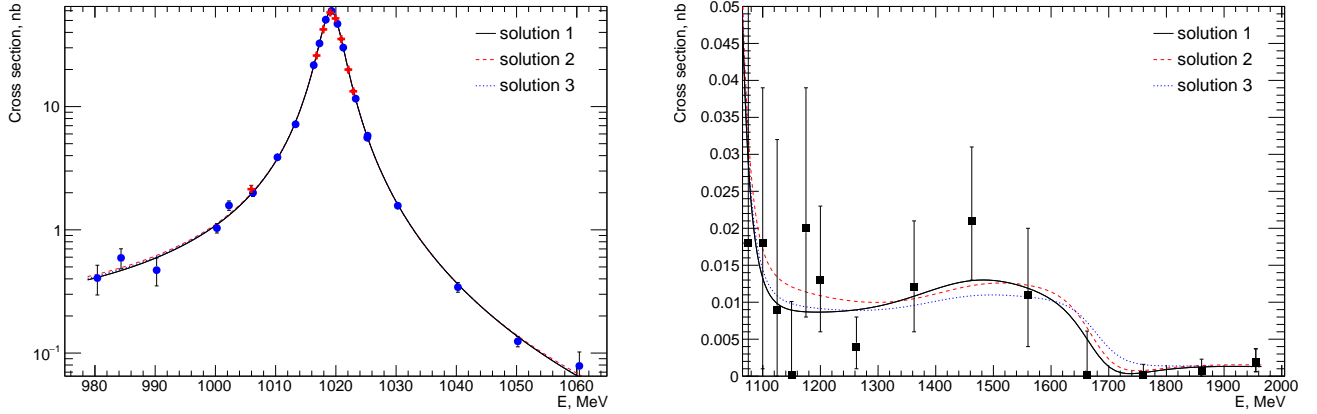


FIG. 4: The Born cross section for the $e^+e^- \rightarrow \eta\gamma$ process. Left panel shows the cross section measured in this work for the 2024 (blue dots) and 2018 (red crosses) energy scans. Right panel shows the cross section measured by SND in Ref. [28]. The black solid, red dashed and blue dotted curves represent the result of the fit described in the text for solution 1, 2, and 3, respectively. The c.m. energy is corrected by the value of the energy scale shift (see Table II).

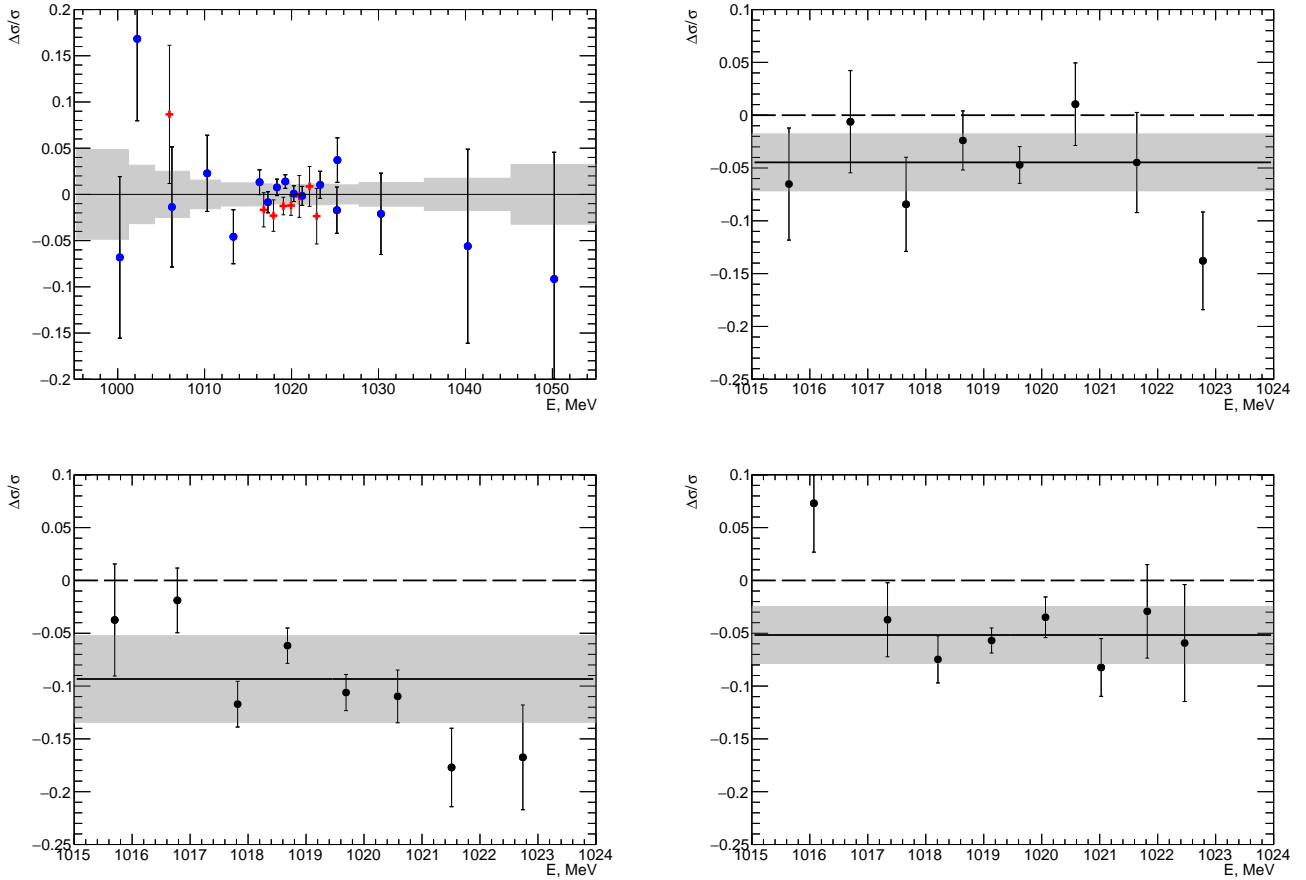


FIG. 5: The relative differences between the measured $e^+e^- \rightarrow \eta\gamma$ Born cross section and the result of the fit described in the text for this work (top left), for the SND measurement using the decay channel $\eta \rightarrow 3\pi^0$ in Ref. [10] (top right), for the CMD-2 measurement in Ref. [12] (bottom left) and for the SND measurement in Ref. [9] (bottom right). The solid line represents the average value of the relative difference. The shaded region represents the systematic uncertainty of corresponding measurement. The c.m. energy for the measurement from this work is corrected by the value of the energy scale shift (see Table II).

equal to its statistical error (Table III) with an additional term corresponding to (6) added in quadrature. The statistical uncertainties of the Born cross section in Table III and in Fig. 4 correspond to the diagonal elements of the obtained covariance matrix. The full correlation matrix is given in the supplementary material.

VII. DISCUSSION

Figure 5 shows the relative differences between the measured $e^+e^- \rightarrow \eta\gamma$ Born cross section and the result of the fit described above for this work and data from Ref. [9, 10, 12]. The solid line on each plot shows the average difference, which is $(-4.5 \pm 1.2 \pm 2.7)\%$ for the SND measurement using the decay channel $\eta \rightarrow 3\pi^0$ in Ref. [10], $(-9.3 \pm 0.9 \pm 4.1)\%$ for the CMD-2 measurement in Ref. [12] and $(-5.2 \pm 0.8 \pm 2.7)\%$ for the SND measurement in Ref. [9]. The first quoted error is statistical and the second is systematic. It is seen that the measurement made in this work has better accuracy and is higher compared to other measurements.

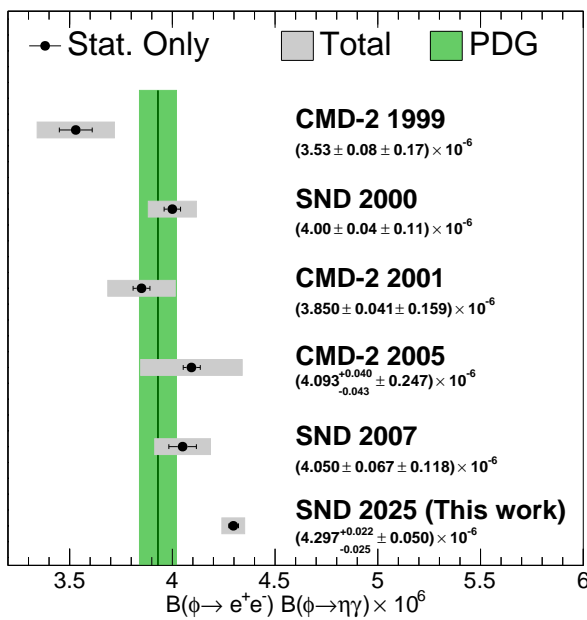


FIG. 6: The value of the branching fractions product $B(\phi \rightarrow e^+e^-)B(\phi \rightarrow \eta\gamma)$ obtained in this work for solution 1 compared to the world average value reported by PDG [25] and to the measurements SND 2007 [10], CMD-2 2005 [13], CMD-2 2001 [12], SND 2000 [9] and CMD-2 1999 [11].

Using the relation $\sigma_\phi = 12\pi B_\phi/m_\phi^2$, where $B_\phi \equiv B(\phi \rightarrow e^+e^-)B(\phi \rightarrow \eta\gamma)$ is the product of the branching fractions of the decays $\phi \rightarrow e^+e^-$ and $\phi \rightarrow \eta\gamma$ and m_ϕ is the ϕ meson mass [25], we can obtain

$$\begin{aligned} B_\phi &= (4.297^{+0.022}_{-0.025} \pm 0.050) \cdot 10^{-6} \quad (\text{solution 1}), \\ B_\phi &= (3.993^{+0.024}_{-0.021} \pm 0.047) \cdot 10^{-6} \quad (\text{solution 2}), \\ B_\phi &= (4.053^{+0.034}_{-0.028} \pm 0.052) \cdot 10^{-6} \quad (\text{solution 3}). \end{aligned}$$

The first error is statistical and the second is systematic. The systematic uncertainty varies depending on the chosen solution. The dominant contribution to it comes from the uncertainty of the measured cross section (1.1-1.2%). Variation of the parameters σ_ρ and Γ_ϕ within their errors is used to estimate corresponding systematic uncertainty, which are 0.4-0.6% and 0.2%, respectively. Since the obtained values for the parameters ΔE_{18} , $\sigma_{\rho'}$, $\varphi_{\rho'}$, $\sigma_{\phi'}$ are largely determined by the data from Ref.[23, 28], their contribution to the total error (0.1-0.3%) is included into the systematic error. The total systematic uncertainty is obtained as a sum in quadrature of all systematic uncertainties from different sources.

Comparison of the obtained product $B(\phi \rightarrow e^+e^-)B(\phi \rightarrow \eta\gamma)$ with the previous measurements makes sense only for the first solution, since the interference pattern between the resonances for other solutions is significantly different from that assumed in previous experimental works. Such a comparison is shown in Fig. 6. Our measurement is higher than all previous ones in accordance with the differences of the measured cross sections discussed above.

VIII. CONCLUSION

In the SND experiment at the VEPP-2000 collider, the measurement of the $e^+e^- \rightarrow \eta\gamma$ cross section has been performed in the center-of-mass energy range from 980 to 1060 MeV. Our measurement is the most accurate to date and is higher compared to other measurements. The total error of the measured cross section at the maximum of the $\phi(1020)$ resonance is 1.5%. From the fit to the cross section data with the vector meson dominance model, the value of the product $B(\phi \rightarrow e^+e^-)B(\phi \rightarrow \eta\gamma)$ has been obtained.

[1] P. O'Donnell, Rev. Mod. Phys. **53**, 673 (1981).
[2] G. Morpurgo, Phys. Rev. D **42**, 1497 (1990).
[3] M. Benayoun, L. Delbuno, and F. Jegerlehner, Eur. Phys. J. C **80**, 81 (2020), [Erratum: Eur.Phys.J.C **80**, 244 (2020)].
[4] R. Escribano and J. Nadal, JHEP **05** (2007), 006.

- [5] F. Ambrosino *et al.* (KLOE Collaboration), JHEP **07** (2009) 105.
- [6] R. Escribano and E. Royo, Phys. Lett. B **807** (2020), 135534
- [7] V. Mathieu, N. Kochelev and V. Vento, Int. J. Mod. Phys. E **18** (2009), 1.
- [8] I. E. Halperin and A. Zhitnitsky, Phys. Rev. D **56** (1997), 7247.
- [9] M. N. Achasov *et al.* (SND Collaboration), Eur. Phys. J. C **12**, 25 (2000).
- [10] M. N. Achasov *et al.* (SND Collaboration), Phys. Rev. D **76**, 077101 (2007).
- [11] R. R. Akhmetshin *et al.* (CMD-2 Collaboration), Phys. Lett. B **460**, 242 (1999).
- [12] R. R. Akhmetshin *et al.* (CMD-2 Collaboration), Phys. Lett. B **509**, 217 (2001).
- [13] R. R. Akhmetshin *et al.* (CMD-2 Collaboration), Phys. Lett. B **605**, 26 (2005).
- [14] M. N. Achasov *et al.*, Nucl. Instrum. Meth. A **449**, 125 (2000).
- [15] V. M. Aulchenko *et al.*, Nucl. Instrum. Meth. A **598**, 102 (2009).
- [16] A. Y. Barnyakov *et al.*, Nucl. Instrum. Meth. A **598**, 163 (2009).
- [17] V. M. Aulchenko *et al.*, Nucl. Instrum. Meth. A **598**, 340 (2009).
- [18] P. Y. Shatunov *et al.* Phys. Part. Nucl. Lett. **13**, 995 (2016).
- [19] E. A. Kuraev and V. S. Fadin, Sov. J. Nucl. Phys. **41**, 466 (1985).
- [20] G. Bonneau and F. Martin, Nucl. Phys. B **27**, 381 (1971).
- [21] J. Allison *et al.* (GEANT Collaboration), Nucl. Instr. Meth. A **835**, 186 (2016).
- [22] E. V. Abakumova *et al.*, Nucl. Instrum. Meth. A **744**, 35 (2014).
- [23] M. N. Achasov *et al.* (SND Collaboration), Phys. Rev. D **110**, no.7, 072001 (2024)
- [24] G. Balossini *et al.*, Phys. Lett. B **663**, 209 (2008).
- [25] S. Navas *et al.* (Particle Data Group), Phys. Rev. D **110**, 030001 (2024).
- [26] N. N. Achasov, M. S. Dubrovin, V. N. Ivanchenko, A. A. Kozhevnikov, and E. V. Pakhtusova, Int. J. Mod. Phys. A **07**, 3187 (1992).
- [27] J. J. Dudek *et al.* [Hadron Spectrum], Phys. Rev. D **88** (2013) no.9, 094505
- [28] M. N. Achasov *et al.* (SND Collaboration), Phys. Atom. Nucl. **86**, no.6, 1157 (2023).
- [29] V. M. Malyshev, arXiv:1505.01509 [physics.data-an].